

# ARCSnake V2: An Amphibious Multi-Domain Screw-Propelled Snake-Like Robot

Sara Wickenhiser<sup>1</sup>, Lizzie Peiros<sup>2</sup>, Calvin Joyce<sup>1</sup>, Peter Gavrillov<sup>1</sup>, Sujaan Mukherjee<sup>1</sup>, Syler Sylvester<sup>2</sup>, Junrong Zhou<sup>1</sup>, Mandy Cheung<sup>2</sup>, Jason Lim<sup>2</sup>, Florian Richter<sup>2</sup>, Michael C. Yip<sup>2</sup> *Senior Member, IEEE*

**Abstract**—Robotic exploration in extreme environments—such as caves, oceans, and planetary surfaces—poses significant challenges, particularly in locomotion across diverse terrains. Conventional wheeled or legged robots often struggle in these contexts due to surface variability. This paper presents ARCSnake V2, an amphibious, screw-propelled, snake-like robot designed for teleoperated or autonomous locomotion across land, granular media, and aquatic environments. ARCSnake V2 combines the high mobility of hyper-redundant snake robots with the terrain versatility of Archimedean screw propulsion. Key contributions include a water-sealed mechanical design with serially linked screw and joint actuation, an integrated buoyancy control system, and teleoperation via a kinematically-matched handheld controller. The robot’s design and control architecture enable multiple locomotion modes—screwing, wheeling, and sidewinding—with smooth transitions between them. Extensive experiments validate its underwater maneuverability, communication robustness, and force-regulated actuation. These capabilities position ARCSnake V2 as a versatile platform for exploration, search and rescue, and environmental monitoring in multi-domain settings.

## I. INTRODUCTION

Robotic exploration in extreme environments, such as caves, oceans and planetary surfaces, poses significant challenges for the diverse set of terrains [1]. Wheeled robots, while energy-efficient on flat surfaces, struggle with uneven or soft terrains due to limited traction and obstacle negotiation capabilities [2]. Humanoid robots, designed to mimic human form and movement, encounter difficulties maintaining balance and robustness in real-world, unpredictable environments, limiting their practical deployment [3]. These limitations underscore the need for more versatile robotic systems capable of traversing multiple domains, including hard ground, granular media, and aquatic environments. Applications such as search and rescue, environmental monitoring, and exploration demand robots that can adapt to varying terrains and overcome obstacles that traditional platforms cannot handle effectively [4], [5].

A promising approach to address these challenges is the development of multi-domain mobile robots that combine different locomotion strategies. One such design is ARCSnake [6] [7], a screw-propelled, snake-like robot that integrates the advantages of screw propulsion with a hyper-

<sup>1</sup>Mechanical and Aerospace Engineering Department, University of California San Diego, La Jolla, CA 92093 USA {swickenhiser, cajoice, pgavrilo, smukherjee, juz058}@ucsd.edu

<sup>2</sup>Electrical and Computer Engineering Department, University of California, San Diego, La Jolla, CA 92093 USA. {epeiros, m3cheung, ssylvester, jk1009, frichter, mlyip}@ucsd.edu



Fig. 1. ARCSnake is a water-sealed, amphibious, screw-propelled, snake-inspired robot for traversing multi-domain environments. It is equipped with a buoyancy control system for underwater stability.

redundant, snake-like backbone. Rotating Archimedean screws have proven effective for propulsion in amphibious and granular media [8], [9], while snake-like robots offer unique locomotive abilities and a compact form factor ideal for navigating confined spaces similar to vine robots [10].

In this work, we present the second iteration of our screw-propelled snake-like robot, ARCSnake V2. ARCSnake V1 achieved many impressive capabilities, but its major

limitation was a lack of underwater capability. While the core concept of using repeated segments paired with U-Joints and screw modules remains similar, we present several key design improvements centered around water based locomotion. The main technical contributions are as follows: a water-proofed mechanical design for serially-linked screw drive train and cable-driven joint actuation, a selective adaptive buoyancy system allowing for depth control and maneuverability underwater, and various locomotion modes on land. Each individual segment is rigorously tested providing the equivalent to IP67 rating for our proposed system. Finally, both a land and an underwater demonstration are conducted to highlight ARCSnakes V2 amphibious capabilities.

## II. RELATED WORKS

### A. Snake Robots

Snakes are uniquely able to navigate and adapt to complex terrains while being extremely structurally simple. This has led to the extensive study of snake-inspired robots that mimic the structure and locomotion patterns of snakes [11]–[13].

The most common type of snake robots consists of a hyper-redundant modular design with actuated joints [14]. Early designs only had one degree of freedom joints, and were able to locomote by utilizing the serpentine gait, which involves actuating joints in a sinusoidal pattern [15]. Most of these robots typically only worked well on flat, rigid ground; however, the same undulating motion can generate propulsion in fluids, and several swimming snake robots were developed using this type of motion [16], [17].

The natural progression towards a higher degree of freedom joints [18] led to significantly increased functionality like climbing stairs [19], [20], climbing up pipes [21], and sidewinding on loose sand [22], [23]. These extra degrees of freedom also allowed control over the normal force and maintaining ground contact, one of the key challenges identified with early snake robot designs [24]–[26].

Real snakes have scales with anisotropic friction properties vital to the efficiency of producing net forward propulsion, which inspired many snake robot designs that utilize passive skins. Examples of passive skins include passive wheels [27]–[30], parallel grooves [31], fins [15], and skates [32].

Passive skin snake robots are often controlled through body-shape changing actuation, in other words, actuating the joints in a specific pattern to mimic the gaits of real snakes, such as serpentine or side-winding. A common technique uses central pattern generators to generate the periodic motions. More sophisticated techniques can utilize sensory feedback to adapt to the environment, such as adaptive stiffness control [33], adaptive sidewinding [22], and obstacle-aided locomotion [34], [35].

A significant advancement in snake robot design is the development of active skins, where actuated mechanisms on the robot’s exterior provide propulsion. This innovation decouples body shape from propulsive action, enabling the robot to move forward while its joints conform to the environment for contact maintenance, grip, or adaptability. Examples of such mechanisms include active wheels [36],

[37], omnidirectional wheels [38], passive rollers on actively rotating bodies akin to Mecanum wheels [39], tank treads [40], [41], toroidal skins [42], and articulated rotors for controlled aerial motions [43], [44]. In contrast, screw-based propulsion systems have demonstrated multi-domain mobility across challenging terrains. Lim et al. [45] showcased the effectiveness of screws in traversing media ranging from sand to dirt. The ARCSnake robot extended this capability by operating efficiently in aquatic environments [7]. The EELS robot, developed for extraterrestrial exploration, has proven the viability of screw-based locomotion on icy terrains [46].

### B. Screw Locomotion

Screw propulsion has been proven as an effective method for locomotion in granular and amphibious environments. Original screw-propelled vehicles were designed for traversing and transporting loads through snow, marshes, sand, and mud [8], [9]. The majority of research into the interaction between rotating screw threads and granular media has consisted of experimental and computational studies [45], [47]–[50], and there have been a few attempts at modeling [47], [51]. These studies confirmed the effectiveness of screw propellers in certain types of media, but also reveal the limitations of screw propulsion. Specifically, screw propulsion performs well in granular media with high shearing forces and low friction, but is ineffective on rigid ground when the screw blades cannot get traction. These studies also explore some of the factors in screw geometry that affect performance, with the most significant factors identified thus far being the lead angle and blade height [47], [51], [52].

The early and most common design for these screw-propelled vehicles and robots consisted of two parallel counter-rotating Archimedes screw rotors [48], [53]–[56]. Some designs instead utilize a series configuration [57], or quad-rotor configuration [58]–[60].

Snake robots and screw propulsion each offer unique advantages for locomotion in complex environments, but neither alone achieves full multi-domain mobility. Although prior work has demonstrated snake-like and screw-propelled motion independently, an integrated, reliable, and amphibious robot remains unrealized. ARCSnake V2 has a fully waterproof design that extends the capabilities of ARCSnake V1 through enhanced joint strength and aquatic functionality, enabling effective locomotion across land, granular media, and underwater environments.

## III. SYSTEM DESIGN

To provide a comprehensive understanding of ARCSnake V2’s design, this section details its key mechanical and electrical components. The ARCSnake system is a modular underwater robot designed for versatile locomotion and control, with key mechanical and electrical components summarized in Table I. Its propulsion relies on a screw actuator with an internal transmission system (Fig. 2), while active joints between segments enable high mobility. Buoyancy is managed through inflatable bladders, and internal pressurization prevents water ingress. The system includes

TABLE I  
SYSTEM SPECIFICATIONS

Specification	Within	Specification Details
Power	Segment	12V-48V, 240W (max)
	System	12V-48V, 960W (max)
Comms	Segment	CAN-BUS
	System	USB and CAN-BUS
Actuator	Screw	Torque: 1.0 Nm Continuous, 3.8 Nm peak
	Half U-Joint	Torque: 2.6 Nm Continuous, 13 Nm peak
Dimensions	Segment	Max Len: 0.441m, Max Dia: 0.269m
	Head	Max Len: 0.252m, Max Dia: 0.190m
	Segment	Max Len: 1.827m, Max Dia: 0.252m
	System	
Buoyancy	Bladders Shells	Torus Shape Foam Filled
Pressurization	Internal Bladders	6 psi 3-5 psig, 3 psia
Waterproof	Rating	IP67

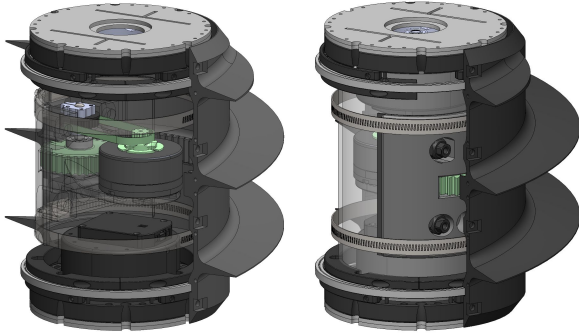


Fig. 2. The images above showcases the screw mechanism. The gear system is shown in green. The left image shows the belt drive which starts with a inner gear mounted to the motor, extending to a pulley connected to the outer gear. As shown in the right image, the outer gear is connected to the screw block's ring gear and meshes with the screwshell, causing the screwshell to rotate with the motor.

distributed power electronics, onboard sensing, and a robust communication interface.

#### A. Mechanical Design

1) *Screw Actuator*: From the exterior, our screw propulsion transmission begins with our 3D printed outer shell. The shell is comprised of two halves that align with each other and a set of thin 6656K17 Ultra-Thin Ball Bearings. Inside the shell at the center is a sun gear which couples with our planetary gear seen in the left image of Fig. 2. The outer gear, which drives the inner gear, is printed out of BambuLabs PLA and installed within the screw transmission block using Spring-Loaded Rotary Shaft Seals, a 5/16" diameter aluminum shaft, and an Active Robotics clamping hub (part 545624). In addition to the gear, this transmission

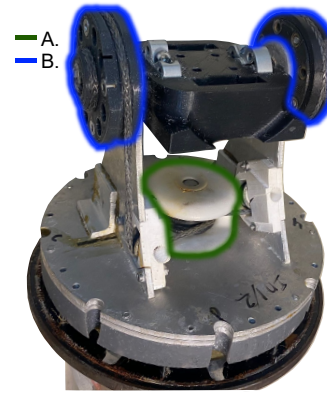


Fig. 3. The U-joint connects screw segments. They are controlled by the U-Joint motor which rotates the input pulley (A.), causing the rope to coil, twisting the output pulley (B.) and changing the angle between the segments. Because of their simple mechanical design, high load rating, and low backlash, timing belts with tension idlers are used for transmission.

block also functions as the pass-through for the power, CAN, and positive pressure lines. The cable penetrators are Blue Robotics WetLink Penetrators, size 4.5 for the CAN line and 8.5 for the power line. The positive pressure line uses a push-to-connect connector with an o-ring seal. Connected to the planetary gear shaft is a 3D-printed pulley with the same embedded 545624 ServoCity shaft clamp. That pulley connects to the sun gear through a belt drive 3D printed pulley directly driven by the screw motor.

2) *U-Joint*: To enable snake-like undulatory locomotion, angle the vector of the screw propulsion, and traverse changes in terrain elevation, ARCSnake V2 incorporates an active universal (U-) joint at each interlink connection. The U-joint provides a hemispherical range of motion, offering over 180° of rotation in both the pitch and yaw axes, which is critical for reproducing the lateral undulations characteristic of snake robots. Each axis is actuated via a cable-driven mechanism powered by an RMD-X8 Pro motor with an internal 5:1 gearbox and an external 1.8:1 reduction, resulting in a continuous torque sufficient to lift an adjacent link. Motor encoders are used for high-resolution position sensing and closed-loop control. The motor is connected to a resin printed pulley that the D12 M-RIG MAX coils around to allow the motor to rotate the U-Joint.

3) *Positive Pressure Line*: A positive pressure line feeds through all segments and supplies 4 psi of pressure. The pressurization makes all seals more robust underwater by releasing air through any cracks instead of allowing water in. This prevents water from entering and damaging the electronics within the segments.

4) *Head Design*: A custom head is designed to enable sample collection and provide front facing video data. It is made out of BambuLabs PLA and has a custom internal 6 bar linkage mechanism that opens the mouth and simultaneously extends a gripper, powered by a 70kg IP68 servo motor. The gripper, from a ROSMASTER M3 Pro Robot, is powered by a 55kg IP68 servo motor able to collect underwater samples



Fig. 4. A torus-shaped bladder is placed around each of the U-Joints with a pressure line attached. This buoyancy system allows for underwater maneuverability and depth control.

of interest as seen in Fig. 7. At the front of the head there is a DJI Action 2 camera with a 135° view positioned to see when the claw has accurately grasped a sample.

### B. Buoyancy System

The Buoyancy System consists of foam-filled screw shells and several Torus-shaped inflatables (referred to as bladders) placed at the U-joints of ARCSnake. Fitting up to two bladders over each U-joint.

To produce an appropriate buoyancy system, the following steps were taken: (1) Initial buoyancy calculations and tests to find the density and buoyant force for each segment, (2) A calculation to determine the passive buoyancy required for the segment buoyancy to be -5%, meaning the segment will slowly sink, (3) A calculation to determine what volume of active buoyancy controlled through air filled bladders was needed to get to 5% buoyant, meaning floating at the surface. (4) The materials and pattern making to ensure a 2D textile would inflate to a desired 3D volume. (5) Subsequent tubing and upstream pressure were designed to work at the surface level and depth, minimizing the chance for bladder rupture.

1) *Buoyancy Calculations:* The system ideally has a buoyancy shift of 5% above and below neutrally buoyant to allow for control of floating, sinking, and swimming. To begin, a calculation was done to ascertain the buoyancy of the segments.

$$F_b = \rho_w g V_{disp} \quad (1)$$

where  $F_b$  is the buoyancy force,  $\rho_w$  the density of water,  $g$  the gravitational constant, and  $V_{disp}$  is the volume of water displaced by the segment. The highest density segments are the middle segments, which have a net force of -19.4 N, making it 72% neutrally buoyant. The other segments (front and tail) without the second half U-joint are both buoyant. In Table II in the mass column, there is an additional number provided, which is the weight added to the segment to make it dense enough to sink.

2) *Flotation Screw Shells:* To add passive buoyancy, the shells were given a larger volume and packed with a 2-part polyurethane Marine Foam. The addition of these shells to

TABLE II  
MASS AND VOLUME DATA

Part	Mass	Volume	Density	Buoyancy
Water	1 kg	1 $m^3$	1000 $\frac{kg}{m^3}$	0 N
Middle Segment	5.386 kg	0.00339 $m^3$	1583.4 $\frac{kg}{m^3}$	-19.4 N
Front Segment + Head	5.006 kg + (1.009) kg	0.004 $m^3$	1,251.5 $\frac{kg}{m^3}$	-39.2 N
Tail Segment	4.486 + (0.796) kg	0.00318 $m^3$	1661.1 $\frac{kg}{m^3}$	-20.6 N
Marine (foam) Shells	1.164 kg	0.00208 $m^3$	559.6 $\frac{kg}{m^3}$	9.0 N
Torus-Shaped Bladder	0.02 kg	0.00143 $m^3$	14.2 $\frac{kg}{m^3}$	13.8 N
Regular Shells	0.544 kg	0.00092 $m^3$	591.3 $\frac{kg}{m^3}$	3.7 N

the middle segments put them at -10.4 N or 84% neutrally buoyant. The size increase of the shells was limited due to the increase in diameter and mass, which negatively impacts the torque of the screw motor. The remaining volume would be handled through the bladders. The shell and the relevant buoyancy information can be found in Table II.

3) *Bladder Volume:* The buoyancy force contributed by each swim bladder is equal to the weight of water displaced, as shown in equation 1. To calculate the buoyancy of the bladders, which are torus-shaped, the Volume equation below was used:

$$V_b = 2\pi^2 r^2 R \quad (2)$$

where  $V_b$  is the total volume for one bladder,  $r$  is the minor diameter of the swim bladder, and  $R$  is the major diameter of the swim bladder.

According to the buoyancy calculations for the middle segments, a buoyancy force of ~10 N is required for neutral buoyancy and ~13.1 N for 5% buoyant. This indicates a target volume required of each bladder to be 0.00143  $m^3$  with a buoyant force of ~13.8 N, adding a 5% buffer to the required buoyant force set point.

4) *Bladder Manufacturing:* Nylon Taffeta Fabric was chosen for fabrication, a waterproof and airtight material ideal for creating the inflatable bladders. One side of the fabric is coated with a thermoplastic, allowing it to be heat-bonded, while the other side is scratch-resistant. This ensures the bladders are resistant to punctures when ARCSnake is traversing through a rocky environment.

The swim bladder is constructed as a flat textile ring that becomes three-dimensional when filled with air. To design a bladder, the change in geometry needs to be accounted for,

$$D_{textile} = D_{major} \pm \frac{\pi}{2} D_{minor} \quad (3)$$

where  $D_{major}$  is the radius of the torus,  $D_{minor}$  is the diameter of the tube that makes up the torus, and  $D_{textile}$  returns the required diameters of the textile ring. This defines



Fig. 5. ARCSnake on various types of land media. From left to right is grass, concrete, mulch, and gravel. ARCSnake is designed to be a multi-domain system.

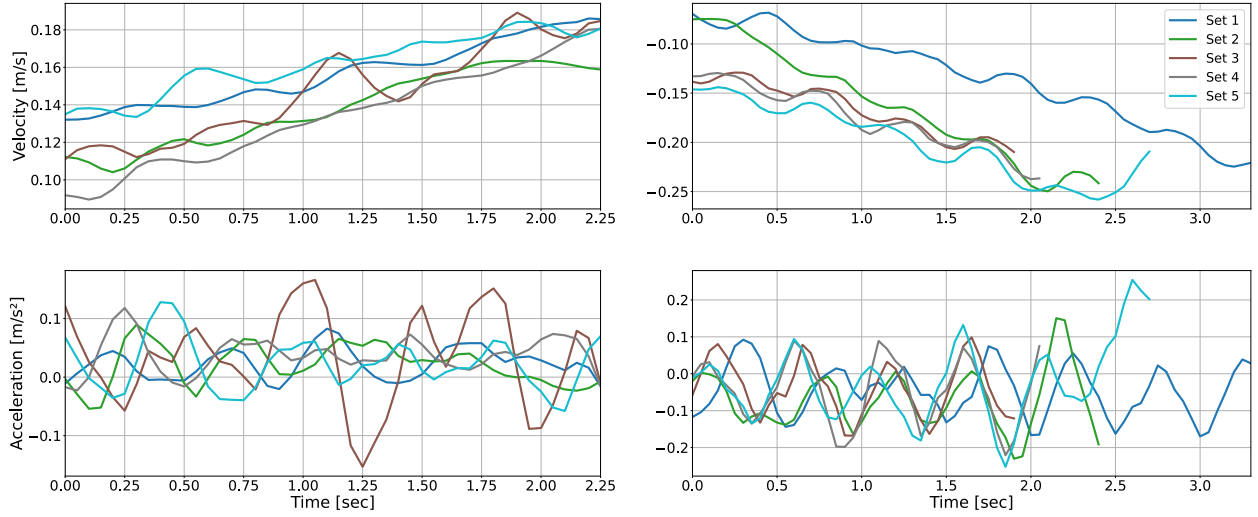


Fig. 6. Rising (left) and falling (right) velocities (top) and accelerations (bottom) for ARCSnake during a portion of the ascent and descent. ARCSnake fell and rose with near constant acceleration due to the buoyancy system.

a flat pattern that is larger in inner and outer diameter, becoming accurate when the volume is pressurized and forms a 3D geometry.

##### 5) Pressure Control System and Theoretical Losses:

Using separate pneumatic lines, the bladders at the front and rear of ARCSnake can be inflated or deflated independently, enabling tilt control underwater. The bladders each have a 6 mm Push-to-Connect Tube Fitting for Air used to connect them into the 6mm OD 2mm ID UV-Resistant Firm Plastic Tubing for Air and Water. The remaining system uses "Y" and straight 6mm push-to-connect fittings from HOODUCTRIC. Upstream pressure is regulated using 2 Bellofram regulators set to 6psi for the positive pressure line and 3-5 psi for the bladders, and a Kobalt Quiet Tech air compressor set to 15 psi tool pressure.

To calculate the necessary upstream limits, both upper and lower, a head loss calculation was done, and a theoretical time to fill was calculated to ensure the bladders would fill within a 60-second time frame. To ensure the bladders settle at 0.15 Bar (2.15 psia), a safe operating pressure for the swim bladders, a minimum upstream pressure of 2.9 psia is required.

As the system is split into two branches (front and back), the total head loss of each branch is needed to decide the required minimum set pressure upstream.

$$h_{Total} = \left( \frac{\rho_a f_D L}{D} + \sum K_i \right) \frac{\bar{v}}{2g} \quad (4)$$

Where  $h_T$  is the total head loss, with all instances of K being various coefficients of minor losses,  $\rho_a$  is the density of air, D is the diameter of the pipe (tubing), L is the length of the pipe (tubing), and  $f_D$  is the friction factor of the pipe.  $\bar{v}$  is the mean velocity at each branch.

##### C. Electronics and Communication

1) *Power Electronics*: Includes power tether, penetrators, and PCB/Converters. The ARCSnake power system comprises a 48V power rail with remote sense and power electronics individually housed in each segment. The 48V power rail is implemented with a BlueRobotics High-Temperature PUR Subsea Cable", P/N BR-101093 cable and BlueRobotics WetLink penetrators for watertight construction. An SJEOW conductor, rated for operating in outdoor and water conditions, is used for remote sensing.

The power electronics individually housed in each segment are managed by a custom-printed circuit board (PCB). The PCB operates a DC-DC converter, VICOR V48B24C250BL, to distribute 24V power from the 48V rail. The U-joint motors associated with each segment are powered directly from the 48V rail. The PCB distributes 24V to the screw shell motor, microcontroller, servo motors, and communication elements.

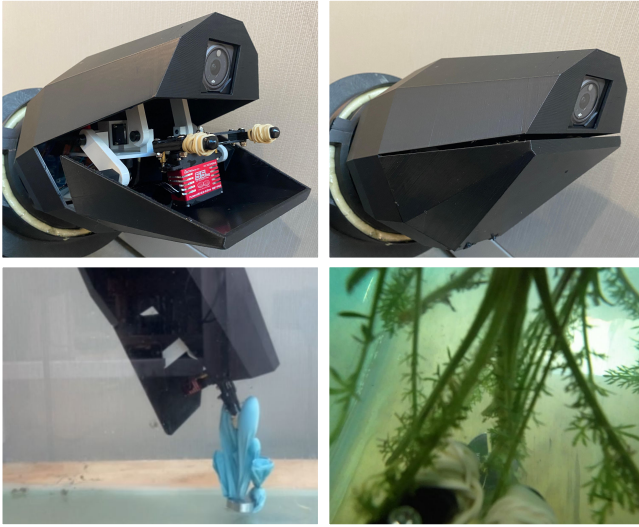


Fig. 7. The top left and right images display ARCSnake's head in open and closed configuration, respectively. The bottom left image shows the head grasping a trash underwater. The bottom right image shows a first person view of the claw collecting a botanical specimen.

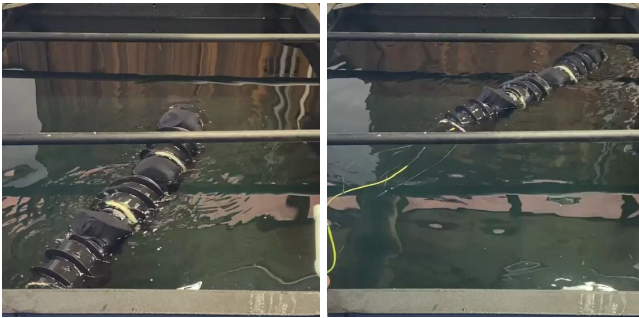


Fig. 8. Starting position (left) and ending position (right) of one of ARCSnake's swims in a water tank. ARCSnake is capable of aquatic movement.

2) *Communication*: The snake communication is based on CANBus where each component (e.g. motors) has a unique address which communicates to the host PC. A Fathom ROV Tether from Blue Robotics was used to connect the CAN line between the PC and the snake system. Between the segments, a waterproof shielded 20 gauge wire was run that enters then exits each segment using the wetlink penetrator from Blue Robotics. In each segment, the CAN line splits to connect with all motors, two or three, depending on whether it is a middle or end segment, and the CANBed - Arduino CAN Bus Dev Kit. The Arduino board is then connected to the internal IMU through I2C, which can be used to gather data on relative motions or angles between the segments or their orientation relative to gravity.

#### IV. EXPERIMENTS

##### A. System Validation

The latency for each CAN node was tested. A round-trip delay from sending a remote desktop command to the first

CAN node and receiving a response was measured at 0.73ms over 1000 samples. This round-trip delay was measured to increase on average by 0.91ms per CAN node along the daisy chain, up to 8.92ms latency.

##### B. Screw Drive Validation

The maximum torque produced by the motor during closed-loop speed control increases with the commanded speed. The peak tangential force measured ranged from 40.0 N to 75.9 N at commanded speeds of 10 rad/s and 50 rad/s, respectively. This corresponds to a resultant torque ranging from 3.60 to 6.83 Nm. Given that the maximum torque output of the motor with no load is about 1.5 Nm and the gear ratio of the screw drive train is 7:1, the ideal resultant torque output at the screw shell should be 10.5 Nm. Thus the efficiency of the screw drive train is calculated to be about 65.7% at a commanded speed of 50 rad/s.

##### C. Buoyancy System Validation

1) *Volume Measurements*: Given the complexity of the inner chamber and U-joint attachments, a water displacement test was used to calculate the volume of the segments. A known volume of water was placed in a regularly shaped container (rectangle), and the height of the water was measured. Then a full middle segment is placed in the water, fully submerged. The new water height was measured. The difference in total volume before and after submerging was used as the segment volume, which is listed in Table II.

2) *Inflation Rate and Headloss Tests*: To test buoyancy, the system was connected to controlled house air with all bladders fully deflated. Both valves were opened simultaneously. The buoyancy system, given an upstream pressure of 2.9 psia, can inflate the bladders in the rear segments in 68 seconds and the bladders in the front segments in 70 seconds. This is a 13.3% error from the desired inflation time. In actual field tests, the upstream pressure was set to 3.0 psia to account for this percent error.

3) *Sinking and Rising*: To test the buoyancy system, the snake was first placed on the water surface with the bladders deflated. The snake was dropped while being filmed from a side-view window. Once the snake reached the bottom, the pressure line to all bladders was opened, and the snake was again filmed rising for post video processing.

The results of the experiment are as follows: When the bladders are deflating, ARCSnake fell with an average acceleration of  $0.045\text{m/s}^2$ . In field testing, ARCSnake took approximately 10 seconds to sink to the bottom of a 1.5-meter water tank. Once at the bottom, the bladders were reinflated with an upstream pressure of 6 psi, and ARCSnake rose with an acceleration of  $0.027\text{m/s}^2$ .

##### D. U-Joint Validation

The U-joint system is validated through a repeatability test, in which the joint follows several periods of a sine-wave trajectory. Varying weights were placed on the end of a half u-joint, and the joint was prescribed a repeated pattern to and from its joint limits to measure hysteresis. The results

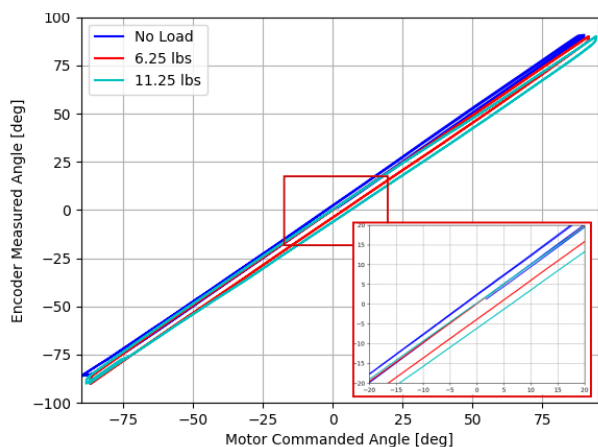


Fig. 9. The graph above depicts the input command vs measures the angle of the motor with varying loads applied. With no load (blue), the hysteresis loop has a width of  $\sim 2$  degrees, at 6.25 lbs (red), the width increases to  $\sim 4$  degrees, and at 11.25 lbs of load (cyan), the width reaches  $\sim 6$  degrees.

are shown in Fig. 9. With no load (blue), the hysteresis loop has a width of  $\sim 2^\circ$ , at 6.25 lbs (red), the width increases to  $\sim 4^\circ$ , and at 11.25 lbs of load (cyan), the width reaches  $\sim 6^\circ$ .

## V. DISCUSSION AND CONCLUSION

This work presents ARCSnake V2, an amphibious, screw-propelled snake-like robot designed for robust locomotion across hard ground, granular media, and aquatic environments. By integrating screw-based propulsion with hyper-redundant joint actuation and a modular, waterproofed architecture, ARCSnake V2 demonstrates effective multi-domain mobility. Experimental results validate its mechanical efficiency, force regulation capabilities, and precise maneuverability in both terrestrial and submerged conditions. ARCSnake was also deployed in a water tank as seen in Fig. 1 and Fig. 8, showcasing its effectiveness in water. Another field test was completed with the head, where the claw grasped aquatic specimen and trash from the bottom of the tank, seen in Fig. 7.

The platform's novel combination of serially linked screw drive segments, cable-driven universal joints, and adaptive buoyancy control enables a diverse set of locomotion modes, supporting its use in unstructured and hazardous environments. These capabilities position ARCSnake V2 as a versatile platform for tasks ranging from sample collection and underwater trash removal to pipe inspection and search-and-rescue missions. For instance, the robot can be deployed to grasp objects on a riverbed with its claw and then use its buoyancy system for retrieval on the surface. Similarly, it can wrap around pipes for inspection while minimizing disruption to surrounding wildlife, and its screw-based propulsion is inherently non-damaging to most surfaces while being less prone to debris entanglement than traditional propeller-driven systems.

Future work will enhance autonomous control strategies through sensor fusion and expanding the platform's scalability for more complex mission profiles. These advancements

aim to further improve the system's adaptability and effectiveness in real-world exploration and intervention tasks.

## VI. ACKNOWLEDGEMENTS

We want to thank Mingwei Yeoh, Colin Brady, Kylie Chan, Andrew Nakoud, Anne-Marie Shui, Yaohui Chen, Zoe Samuels, Diego Williams, Tarun Murugesan, Derek Chen, Dimitri Schreiber, Hoi Man (Kevin) Lam, and Casey Price for their contributions.

## REFERENCES

- [1] H. Kalita and J. Thangavelautham, "Exploration of extreme environments with current and emerging robot systems," *Current Robotics Reports*, vol. 1, no. 3, pp. 97–104, 2020.
- [2] L. Bruzzone and G. Quaglia, "Review article: locomotion systems for ground mobile robots in unstructured environments," *Mechanical Sciences*, vol. 3, pp. 49–62, 2012.
- [3] W. Zhang, M. Li, and Y. Chen, "Motion planning and control with environmental uncertainties for humanoid robot," *Sensors*, vol. 24, no. 23, p. 7652, 2024.
- [4] C. Li and K. Lewis, "The need for and feasibility of alternative ground robots to traverse sandy and rocky extraterrestrial terrain," *Advanced Intelligent Systems*, vol. 4, no. 3, p. 2100195, 2022.
- [5] J. P. Queralta, J. Taipalmaa, B. C. Pullinen, V. K. Sarker, T. N. Gia, H. Tenhunen, M. Gabbouj, J. Raitoharju, and T. Westerlund, "Collaborative multi-robot systems for search and rescue: Coordination and perception," *arXiv preprint arXiv:2008.12610*, 2020.
- [6] D. A. Schreiber, F. Richter, A. Bilan, P. V. Gavrilo, H. M. Lam, C. H. Price, K. C. Carpenter, and M. C. Yip, "Arcsnake: an archimedes' screw-propelled, reconfigurable serpentine robot for complex environments," in *2020 IEEE International Conference on Robotics and Automation (ICRA)*, pp. 7029–7034, IEEE, 2020.
- [7] F. Richter, P. V. Gavrilo, H. M. Lam, A. Degani, and M. C. Yip, "Arcsnake: Reconfigurable snakelike robot with archimedean screw propulsion for multidomain mobility," *IEEE Transactions on Robotics*, vol. 38, no. 2, pp. 797–809, 2021.
- [8] M. Neumeyer and B. Jones, "The marsh screw amphibian," *Journal of Terramechanics*, vol. 2, no. 4, pp. 83–88, 1965.
- [9] H. Dugoff and I. Robert Ehlich, "Model tests of bouyant screw rotor configurations," *Journal of Terramechanics*, vol. 4, no. 3, pp. 9–22, 1967.
- [10] M. M. Coad, L. H. Blumenschein, S. Cutler, J. A. R. Zepeda, N. D. Naclerio, H. El-Hussieny, U. Mehmood, J.-H. Ryu, E. W. Hawkes, and A. M. Okamura, "Vine robots," *IEEE Robotics & Automation Magazine*, vol. 27, no. 3, pp. 120–132, 2019.
- [11] S. Hirose, *Biologically Inspired Robots*. Oxford University Press Inc., 1992.
- [12] S. Hirose and M. Mori, "Biologically inspired snake-like robots," in *2004 IEEE International Conference on Robotics and Biomimetics*, pp. 1–7, IEEE, 2004.
- [13] A. A. Transteth, K. Y. Pettersen, and P. Liljeback, "A survey on snake robot modeling and locomotion," *Robotica*, vol. 27, pp. 999–1015, Dec 2009.
- [14] C. Wright, A. Johnson, A. Peck, Z. McCord, A. Naaktgeboren, P. Gianfortoni, M. Gonzalez-Rivero, R. Hatton, and H. Choset, "Design of a modular snake robot," in *IEEE/RSJ International Conference on Intelligent Robots and Systems*, pp. 2609–2614, IEEE, 2007.
- [15] S. Hirose and H. Yamada, "Snake-like robots [tutorial]," *IEEE Robotics & Automation Magazine*, vol. 16, no. 1, pp. 88–98, 2009.
- [16] A. Crespi and A. J. Ijspeert, "Amphibot ii: An amphibious snake robot that crawls and swims using a central pattern generator," in *Proceedings of the 9th international conference on climbing and walking robots*, pp. 19–27, 2006.
- [17] N. Kamamichi, M. Yamakita, K. Asaka, and Z.-W. Luo, "A snake-like swimming robot using ipmc actuator/sensor," in *IEEE International Conference on Robotics and Automation*, pp. 1812–1817, IEEE, 2006.
- [18] E. Shammas, A. Wolf, and H. Choset, "Three degrees-of-freedom joint for spatial hyper-redundant robots," *Mechanism and machine theory*, vol. 41, no. 2, pp. 170–190, 2006.
- [19] M. Nakajima, M. Tanaka, K. Tanaka, and F. Matsuno, "Motion control of a snake robot moving between two non-parallel planes," *Advanced Robotics*, vol. 32, pp. 1–15, 2018.

- [20] Y. Iguchi, M. Nakajima, R. Ariizumi, and M. Tanaka, "Step climbing control of snake robot with prismatic joints," *Sensors*, vol. 22, no. 13, p. 4920, 2022.
- [21] F. Trebuña, I. Virgala, M. Pástor, T. Lipták, and L. Miková, "An inspection of pipe by snake robot," *International Journal of Advanced Robotic Systems*, vol. 13, no. 5, pp. 1–12, 2016.
- [22] H. Marvi, C. Gong, N. Gravish, H. Astley, M. Travers, R. L. Hatton, J. R. Mendelson, H. Choset, D. L. Hu, and D. I. Goldman, "Sidewinding with minimal slip: Snake and robot ascent of sandy slopes," *Science*, vol. 346, no. 6206, pp. 224–229, 2014.
- [23] C. Gong, M. Tesch, D. Rollinson, and H. Choset, "Snakes on an inclined plane: Learning an adaptive sidewinding motion for changing slopes," *2014 IEEE/RSJ International Conference on Intelligent Robots and Systems*, pp. 1114–1119, 2014.
- [24] S. Ma, "Analysis of creeping locomotion of a snake-like robot," *Advanced Robotics*, vol. 15, no. 2, pp. 205–224, 2001.
- [25] S. Ma and N. Tadokoro, "Analysis of creeping locomotion of a snake-like robot on a slope," *Autonomous Robots*, vol. 20, no. 1, pp. 15–23, 2006.
- [26] Z. Y. Bayraktaroglu, A. Kilicarslan, A. Kuzucu, V. Hugel, and P. Blazevic, "Design and control of biologically inspired wheel-less snake-like robot," in *The First IEEE/RAS-EMBS International Conference on Biomedical Robotics and Biomechanics*, pp. 1001–1006, IEEE, 2006.
- [27] C. Ye, S. Ma, B. Li, and Y. Wang, "Turning and side motion of snake-like robot," in *IEEE International Conference on Robotics and Automation, 2004. Proceedings. ICRA'04. 2004*, vol. 5, pp. 5075–5080, IEEE, 2004.
- [28] A. Crespi, A. Badertscher, A. Guignard, and A. J. Ijspeert, "Amphibot i: an amphibious snake-like robot," *Robotics and Autonomous Systems*, vol. 50, no. 4, pp. 163–175, 2005.
- [29] X. Wu and S. Ma, "Cpg-based control of serpentine locomotion of a snake-like robot," *Mechatronics*, vol. 20, no. 2, pp. 326–334, 2010.
- [30] Z. Cao, Q. Xiao, R. Huang, and M. Zhou, "Robust neuro-optimal control of underactuated snake robots with experience replay," *IEEE transactions on neural networks and learning systems*, vol. 29, no. 1, pp. 208–217, 2017.
- [31] M. Saito, M. Fukaya, and T. Iwasaki, "Serpentine locomotion with robotic snakes," *IEEE Control Systems*, vol. 22, no. 1, pp. 64–81, 2002.
- [32] G. Endo, K. Togawa, and S. Hirose, "A self-contained and terrain-adaptive active cord mechanism," *Advanced Robotics*, vol. 13, no. 1, pp. 243–244, 1999.
- [33] D. Zhang, H. Yuan, and Z. Cao, "Environmental adaptive control of a snake-like robot with variable stiffness actuators," *IEEE/CAA Journal of Automatica Sinica*, vol. 7, no. 3, pp. 745–751, 2020.
- [34] A. A. Transeth, R. I. Leine, C. Glocker, K. Y. Pettersen, and P. Liljebäck, "Snake robot obstacle-aided locomotion: Modeling, simulations, and experiments," *IEEE Transactions on Robotics*, vol. 24, no. 1, pp. 88–104, 2008.
- [35] P. Liljebäck, K. Y. Pettersen, Ø. Stavdahl, and J. T. Gravdahl, "Experimental investigation of obstacle-aided locomotion with a snake robot," *IEEE Transactions on Robotics*, vol. 27, no. 4, pp. 792–800, 2011.
- [36] B. Klaassen and K. L. Paap, "Gmd-snake2: a snake-like robot driven by wheels and a method for motion control," in *IEEE International Conference on Robotics and Automation*, vol. 4, pp. 3014–3019, IEEE, 1999.
- [37] H. Date, Y. Hoshi, and M. Sampei, "Locomotion control of a snake-like robot based on dynamic manipulability," in *IEEE/RSJ International Conference on Intelligent Robots and Systems*, pp. 2236–2241, IEEE, 2000.
- [38] C. Ye, S. Ma, B. Li, and Y. Wang, "Modular universal unit for a snake-like robot and reconfigurable robots," *Advanced Robotics*, vol. 23, no. 7-8, pp. 865–887, 2009.
- [39] H. Fukushima, S. Satomura, T. Kawai, M. Tanaka, T. Kamegawa, and F. Matsuno, "Modeling and control of a snake-like robot using the screw-drive mechanism," *IEEE Transactions on Robotics*, vol. 28, no. 3, pp. 541–554, 2012.
- [40] M. A. Armada, G. Granosik, M. G. Hansen, and J. Borenstein, "The omnitread serpentine robot for industrial inspection and surveillance," *Industrial Robot: An International Journal*, vol. 32, no. 2, pp. 139–148, 2005.
- [41] J. Borenstein, M. Hansen, and A. Borrell, "The omnitread ot-4 serpentine robot—design and performance," *Journal of Field Robotics*, vol. 24, no. 7, pp. 601–621, 2007.
- [42] J. C. McKenna, D. J. Anhalt, F. M. Bronson, H. B. Brown, M. Schwestern, E. Shamma, and H. Choset, "Toroidal skin drive for snake robot locomotion," in *IEEE International Conference on Robotics and Automation*, pp. 1150–1155, IEEE, 2008.
- [43] M. Zhao, T. Anzai, F. Shi, X. Chen, K. Okada, and M. Inaba, "Design, modeling, and control of an aerial robot dragon: A dual-rotor-embedded multilink robot with the ability of multi-degree-of-freedom aerial transformation," *IEEE Robotics and Automation Letters*, vol. 3, no. 2, pp. 1176–1183, 2018.
- [44] M. Zhao, F. Shi, T. Anzai, K. Chaudhary, X. Chen, K. Okada, and M. Inaba, "Flight motion of passing through small opening by dragon: Transformable multilinked aerial robot," in *IEEE/RSJ International Conference on Intelligent Robots and Systems*, pp. 4735–4742, IEEE, 2018.
- [45] J. Lim, C. Joyce, E. Peiros, M. Yeoh, P. V. Gavrilo, S. G. Wickenhiser, D. A. Schreiber, F. Richter, and M. C. Yip, "Mobility analysis of screw-based locomotion and propulsion in various media," in *2023 IEEE International Conference on Robotics and Automation (ICRA)*, pp. 7317–7323, IEEE, 2023.
- [46] K. Carpenter, A. Thoesen, D. Mick, J. Martia, M. Cable, K. Mitchell, S. Hovsepian, J. Jasper, N. Georgiev, R. Thakker, A. Kourchians, B. Wilcox, M. Yip, and H. Marvi, *Exobiology Extant Life Surveyor (EELS)*, pp. 328–338. ASCE Library, 2021.
- [47] A. M. Group and B. N. Cole, "Inquiry into amphibious screw traction," *Proceedings of the Institution of Mechanical Engineers*, vol. 175, p. 919–940, June 1961.
- [48] H. Dugoff and I. R. Ehlich, "Model tests of bouyant screw rotor configurations," *Journal of Terramechanics*, vol. 4, no. 3, pp. 9–22, 1967.
- [49] A. Thoesen, S. Ramirez, and H. Marvi, "Screw-generated forces in granular media: Experimental, computational, and analytical comparison," *AICHE Journal*, vol. 65, no. 3, p. 894–903, 2019.
- [50] K. Matsuhiro, K. Tanaka, S. Inoue, T. Zhong, K. Kida, Y. Sugahara, A. Takanishi, and H. Ishii, "Development of small robot with inline archimedean screw mechanism that can move through wetlands," in *ROMANSY 23 - Robot Design, Dynamics and Control* (G. Venture, J. Solis, Y. Takeda, and A. Konno, eds.), (Cham), pp. 338–346, Springer International Publishing, 2021.
- [51] K. Nagaoka, M. Otsuki, T. Kubota, and S. Tanaka, "Terramechanics-based propulsive characteristics of mobile robot driven by archimedean screw mechanism on soft soil," in *IEEE/RSJ International Conference on Intelligent Robots and Systems*, pp. 4946–4951, IEEE, 2010.
- [52] C. Joyce, J. Lim, R. Nguyen, M. Owens, S. Wickenhiser, E. Peiros, F. Richter, and M. C. Yip, "Nasu—novel actuating screw unit: Origami-inspired screw-based propulsion on mobile ground robots," *arXiv preprint arXiv:2310.00184*, 2023.
- [53] W. Fales, D. W. Amick, and B. G. Schreiner, "The riverine utility craft (ruc)," *Journal of Terramechanics*, vol. 8, no. 3, pp. 23–38, 1972.
- [54] K. Nagaoka, M. Otsuki, T. Kubota, and S. Tanaka, "Development of lunar exploration rover using screw propulsion units: Note on dynamic behavior and moving direction control," in *Proc. 19th Workshop on JAXA Astrodyn. Flight Mech*, pp. 143–148, 2009.
- [55] D. Osiński and K. Szykiedans, "Small remotely operated screw-propelled vehicle," in *Progress in Automation, Robotics and Measuring Techniques*, pp. 191–200, Springer, 2015.
- [56] D. He and L. Long, "Design and analysis of a novel multifunctional screw-propelled vehicle," in *International Conference on Unmanned Systems*, pp. 324–330, IEEE, 2017.
- [57] J. H. Lugo, M. Zoppi, and R. Molfino, "Design and kinematic modeling of a screw-propelled mobile robot to perform remote explosive scent tracing filter sampling in forest during humanitarian demining," in *Advances in Cooperative Robotics*, pp. 699–715, World Scientific, 2017.
- [58] J. T. Freeberg, "A study of omnidirectional quad-screw-drive configurations for all-terrain locomotion," 2010.
- [59] J. H. Lugo, V. Ramadoss, M. Zoppi, and R. Molfino, "Conceptual design of tetrad-screw propelled omnidirectional all-terrain mobile robot," in *2nd International Conference on Control and Robotics Engineering*, pp. 13–17, IEEE, 2017.
- [60] O. Oladunjoye, C. Maffattone, J. Al-Nawal, S. Fasullo, E. Greenspan, J. Koller, A. Nikulin, T. de Smet, and G. M. Clayton, "Omnidirectional all-terrain screw-driven robot design, modeling, and application in humanitarian demining\*," *IFAC-PapersOnLine*, vol. 55, no. 27, pp. 7–12, 2022. 9th IFAC Symposium on Mechatronic Systems MECHATRONICS 2022.